Finite element modelling of an asynchronous motor with one broken rotor bar, comparison with the data recorded on a prototype and material aspects

S. Guérard
Montéfiore Inst., Dept. TDEE
University of Liège
s.guerard@ulg.ac.be

J. Gyselinck
Maître de conférence at ULg until 31 July 2004
At present chargé de cours at the ULB
johan.gyselinck@ulb.ac.be

J. Lecomte-Beckers
Dept. ASMA, Matériaux Métalliques Spéciaux
University of Liège
jacqueline.lecomte@ulg.ac.be

Lauréate du prix Melchior Salier 2004 du meilleur travail de fin d'études — section électromécanique-énergétique

Abstract

This work studies the problem of broken rotor bars in cage induction motors. To this aim, an induction machine from WEG Motors was modelled by means of the finite element method. The motor modelled is a 18.5kW four-pole induction motor with a straight rotor cage. The field distribution and stator phase currents were computed for a motor without broken rotor bars and for a motor with one broken rotor bar. The computed stator phase currents were compared to the ones recorded on motors with respectively no broken rotor bar and with one broken rotor bar. The FE model and an equivalent scheme of the motor permitted to show that the resistance of the rotor cage was higher than expected, considering only the temperature effect on the conductivity of the rotor bars. A metallurgic analysis of the aluminium alloy of two rotor bars revealed the presence of a very high density of rich silicon and silicon oxide inclusions, as well as the presence of shrinkages and cracks, which have a negative impact on both conductivity and mechanical strength. A corrected value of the rotor bar conductivity was used in the finite element model and led to a good agreement with the experimental results. The field perturbation associated with a broken rotor bar produces a concentration of flux near the bar ahead of the broken one, considering the counterclockwise direction of rotation of the rotor. This flux concentration results in higher current values –and hence in higher stresses– in the bar ahead of the broken one.

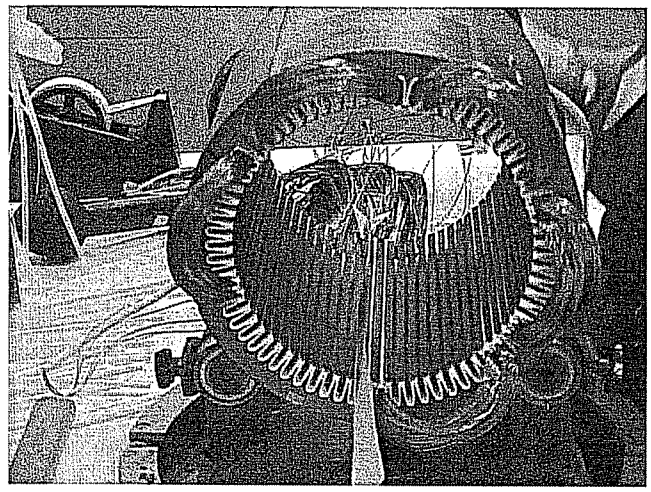

Figure 1: The windings are placed in slots around the inner periphery of the stator

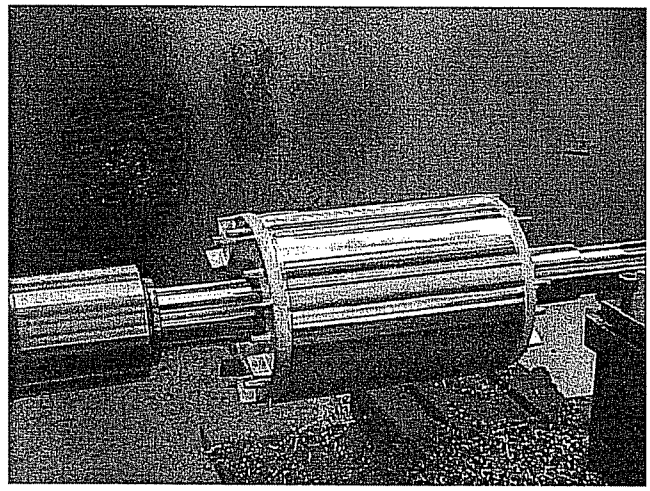

Figure 2: Cage rotor is being turned in order to obtain a constant-width air-gap

1 Introduction

1.1 The induction motor

In its most common form, an induction machine has a cylindrical stator with a laminated magnetic circuit and a three-phase distributed winding, usually placed symmetrically in slots around its inner periphery (see figure 1).
A constant-width air-gap separates the stator from the rotor.

The rotor has a laminated magnetic circuit as well and is characterized by its conductor type which can be massive –for a cage rotor– or wound. The rotor being submitted to various stresses, cage rotors are often preferred to wound rotors for their robustness. Figure 2 shows a cage rotor once it is rectified (to obtain a constant width air-gap). Let us now define the induction machine parameters. Let $\dot{\theta}$ (rad/s) be the rotor revolution speed. This speed is often defined as a function of the slip s:

$$\dot{\theta} = (1 - s)\frac{\omega}{p},$$

where $\omega = 2 \cdot \pi \cdot f$ and p is the number of pole pairs, f being the frequency (Hz).

- When $s = 1$, the rotor is at standstill,
- When $s = 0$, the rotor is running at the synchronous speed.

The slip is hence a measure of the relative difference between the rotor revolution speed and the synchronous speed. Since rotor electromotive forces can only be generated if the rotor is submitted to a variable magnetic field, a torque will be generated for any slip value different from zero, i.e. for any rotor revolution speed $\dot{\theta}$ different from $\dot{\theta}_s = \frac{\omega}{p}$. That is where the asynchronous denomination comes from.
Generally, the bars of the rotor cage are skewed. Originally, the technique was used to provide starting torque when the rotor had the same number of slots as the stator [1]. Because of its positive impact on the reduction of harmonics, the technique was kept even after starting torque was provided by choosing an adequate combination of rotor and stator slot numbers. Figures 3 and 4 show harmonic tables of a skewed cage machine and a straight cage machine respectively. One can notice a decrease in the presence of harmonics 2, 5, 11 and in higher order harmonics.

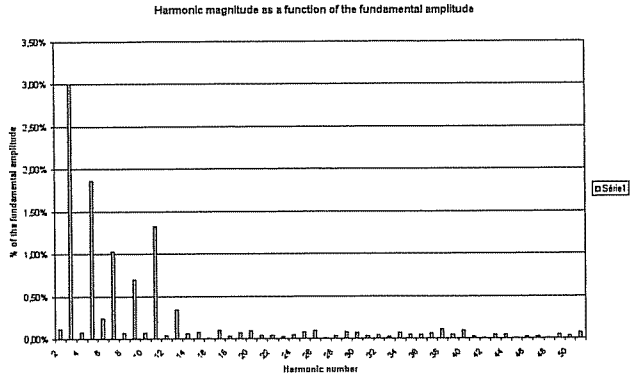

Figure 3: Harmonic table of skewed rotor motor at rated load

Skewing also influences other characteristics of the motor.

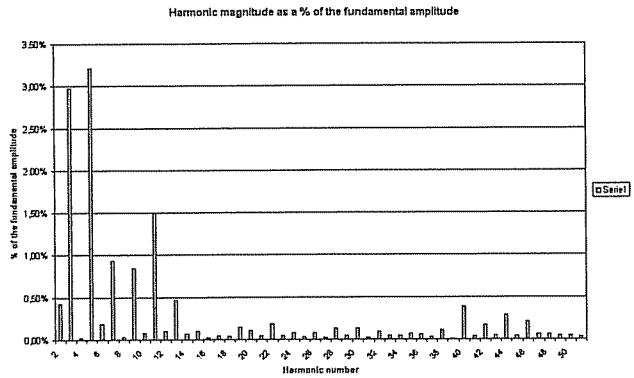

Figure 4: Harmonic table of no-skew rotor motor at rated load

A motor having a skewed rotor always has a slightly higher leakage reactance (5% to 10% is typical) –and therefore somewhat lower torque– than one without skew [2]. By reducing the harmonic current, skewing also lowers the noise output level. Another consequence of induction motor skew is the rise in inter-bar currents. Inter-bar currents are parasitic currents which presence is due to the absence of perfect insulation between the cage and the core.[3]
In this paper, only straight cage motors are considered. As explained in section 3, this allows us to use a 2D finite element model.

1.2 Broken rotor bars

When a motor is running, it is submitted to different kinds of mechanical stresses. Since the rotor is made of two different materials, namely iron laminations and aluminium –sometimes copper– rotor bars, it is submitted to a differential expansion which induces stresses when its temperature rises. The high starting currents might cause a consequent temperature elevation, the rotor thus being subjected to thermal wear. When present, static or dynamic eccentricities of the rotor induce vibrations and thus stresses on the rotor [4]. Electromagnetic stresses, residual stresses, dynamic and mechanical stresses, are also acting on the motor. All these stresses acting together on the motor might lead to a failure of a rotor bar.
The quality of manufacturing process (particularly during the die-casting process of the rotor cage) is an important factor to provide a longer life-time to rotor bars. In the literature, many articles are devoted to the detection of broken bars [5-9]. The presence of broken bars has an impact on losses, slip, efficiency, rated temperature and noise. Let us call I_a the line current, P_a the absorbed power, $\cos\phi$ the load factor, P_{j1} the stator losses, P_{j2} the rotor losses, P_{tot} the total losses, RPM the revolution speed, T the torque and ΔT the temperature rise of the motor frame. In table 1, we compare the characteristics of motors with straight bars at rated load, when the number of broken bars (N) increases (the

rotor cage consists of 40 bars). The data was recorded at WEG Brazil in February and March 2004, according to the separated loss measurement method. (In order to obtain "broken bars", respectively 1, 8, or 16 rotor slots of the injection mold were obstructed during the die-casting process.)

Table 1–Characteristics of a straight cage motor when the number of broken bars increases

N	0	1	8	16
I_a (A)	31.96	32.48	33.76	36.70
P_a (W)	20278	20483	20859	21687
$\cos(\phi)$	0.831	0.827	0.809	0.775
P_{j1} (W)	729.05	748.19	847.6	1089.49
$P_{j2}(W)$	462.82	464.43	625.97	994.78
$P_{tot}(W)$	1978	2083	2459	3287
RPM	1756	1757	1743	1713
T (kgf.m)	10.14	10.18	10.22	10.44
$\Delta T(°C)$	40.71	49.26	41.50	64.55

Analyzing the table, we see the amount of power absorbed by the motor increases with the number of broken bars, and so do rotor losses and frame temperature variation. The increase in the number of broken bars results in more slip, and hence in a lower revolution speed. The load factor decreases as well.

Monitoring these parameters can give valuable qualitative information on the presence of broken rotor bars.

Let us now consider the impact of one broken bar on the current harmonic spectrum of a straight cage motor (see figure 5).

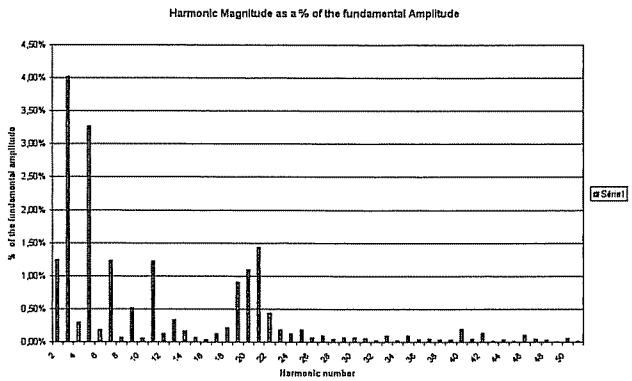

Figure 5: Harmonic spectrum of a straight cage motor with one broken bar

Comparing this figure with figure 4, we observe that some peaks have appeared in harmonics 19, 20 and 21. As a consequence, an harmonic analysis permits to detect the presence of one broken bar in a straight cage motor. As for the skewed cage rotors, the influence of broken bar harmonics is not so obvious because of the damping action of skew on harmonics.

2 Finite Element Model

2.1 The induction motor

We consider a 4-pole IP55 three-phase motor from WEG Motores, with a 60Hz frequency and straight slots. Other characteristics are:

- rated power: 18.5 kW,
- rated speed: 1760 rpm,
- rated voltage: 220 V,
- rated current: 64.3A,
- 91% efficiency at rated power,
- weight: 125 kg.

Figure 6 shows the cage of the motor studied.

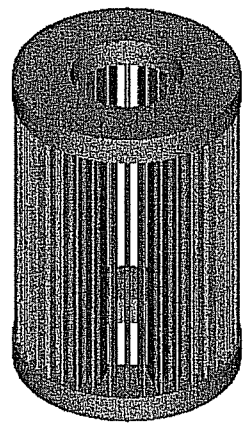

Figure 6: Rotor cage of the motor modelled

2.2 Hypotheses and construction of a model

The motor is modelled under the following hypotheses:

- the problem is considered as dynamic, since there are induced currents in the rotor cage; skin effect is taken into account,
- a 2D magnetic field is assumed in the straight cage rotor motor,
- saturation of the stator and rotor laminations is taken into account, which leads to a non-linear problem.

A classical magnetic vector potential formulation is used [12]. The softwares used are Gmsh and GetDP, respectively to generate the geometry and mesh and to compute solutions [12]. A picture of the one pole model and its mesh can be seen in figures 7 and 8.

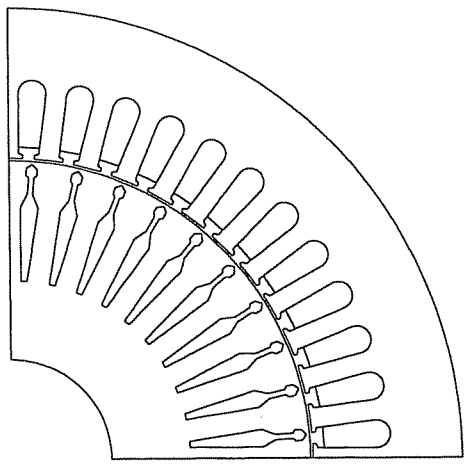

Figure 7: Geometry of the one-pole model

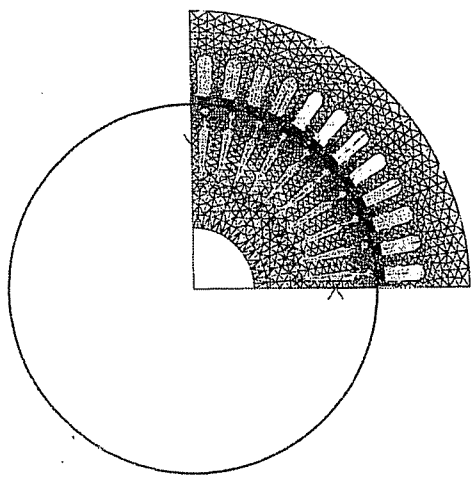

Figure 8: Mesh of the one-pole model

In order to render the rotational motion of the rotor, it is slightly shifted around its axe at each time step, and the layer of finite elements connecting stator and rotor is meshed again (see figure 9).

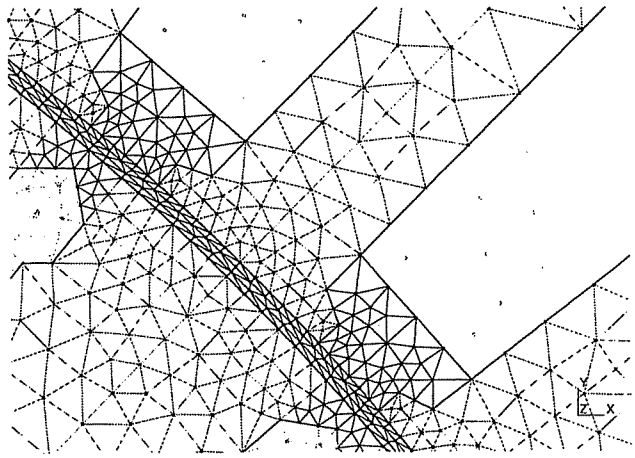

Figure 9: Zoom on the one pole model mesh. The mesh of the air-gap visible

The spatial integration scheme is a Gauss scheme with one integration point. The differential equations are solved in the time domain by means of a simple backward Euler scheme.

2.3 Characteristics of the rotor cage

The alloy used to die-cast rotor cages is a 99.7% weight purity alloy. According to the data supplied by WEG Motores, the alloying elements are:

- Si (max. 0.2%)
- Fe (max. 0.25%)
- Cu (max. 0.01%)
- Zn (max. 0.04%)
- Ti (max. 0.02%),

and the conductivity at $20°C$ is $34.5 \cdot 10^6$ S/m.
When the motor is running, a heat flux is generated, mainly by Joule effect, but hysteresis losses and eddy current losses are also present. This heat flux generates a temperature rise in the motor, and therefore a rise in the resistance of the rotor bars. Frame temperature measurements were made during the tests. A temperature of $65°C$ was recorded for rated load with no broken bars. This temperature kept rising as the number of broken bars grew (up to $90°C$ with 16 broken bars). $80°C$was taken as a rough estimation of the average temperature in the rotor bars. The hypothesis that the temperature coefficient was constant and equal to $0.0039(1/°K)$over the temperature range was made. In the FE model, the temperature rise is simulated by entering a corrected value for the conductivity: $28 \cdot 10^6$S/m.

The rotor cage is ended by two end-rings. The end-ring segment parameters required for the finite element model, namely their resistance and inductance, are estimated analytically [13]. The following pictures show the anti-periodical rotor circuit of the one pole model (figure 10), and the periodical circuit of the four pole model (figure 11). In the rotor circuit which is used for the one-pole model, anti-periodicity is imposed.

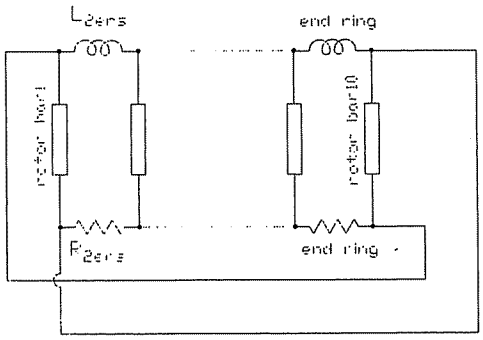

Figure 10: Rotor circuit of the one pole model

Only ten rotor bars out of forty are included in the model. The rotor bars are separated at one end by the end-ring inductance of one segment of rotor cage, and by the end-ring resistances at the other end. In the rotor circuit which is used for the four-pole model, periodicity is imposed.

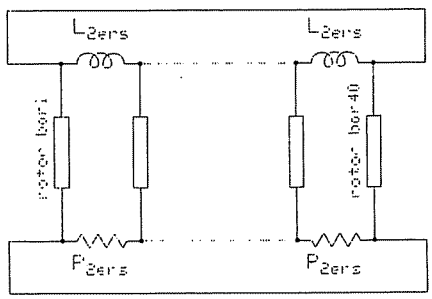

Figure 11: Rotor circuit of the four-pole model

The forty rotor bars are modelled.

3 Material aspects

3.1 Density of the rotor bars

A density measurement of rotor bars was carried out at the MMS (Matériaux Métalliques Spéciaux) laboratory, University of Liège with samples provided by WEG Motores. The samples come from an induction motor which was plunged in acid in order to dissolve the laminations. The density of the rotor bars was measured by double weighing them, once in water, the other time in air. An hypothesis test showed that there were two populations in the rotor bars. The average density of the first group (one fifth of the bars) is 2.61, the average density of the second group is 2.49, while the density of the alloy is 2.7. Actually, the denser bars are always located under the die casting injection points. Cutting the rotor bars into three pieces as shown in figure 12, the density analysis shows the middle of the bar is less dense than its extremities (about 1%), which shows that molten metal feeding during injection is difficult at this location.

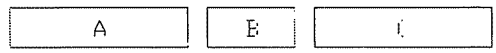

Figure 12: The rotor bars are cut in three pieces to measure the difference of density along the bar

3.2 Metallographic microscope analysis

Micrographies of the alloy were made at the MMS laboratory. The preparation of the sample is explained in [12]. A failure in liquid metal feeding can be seen in figure 13, clinks in figure 14 and a very dense presence of inclusions on all the samples. What is remarkable is that these inclusions are surrounded by a void (see for example figure 16). Moreover, the shape of the inclusion follows the matrix hole contour, which leads to believe that the inclusions were trapped in the aluminum matrix during the solidification process.

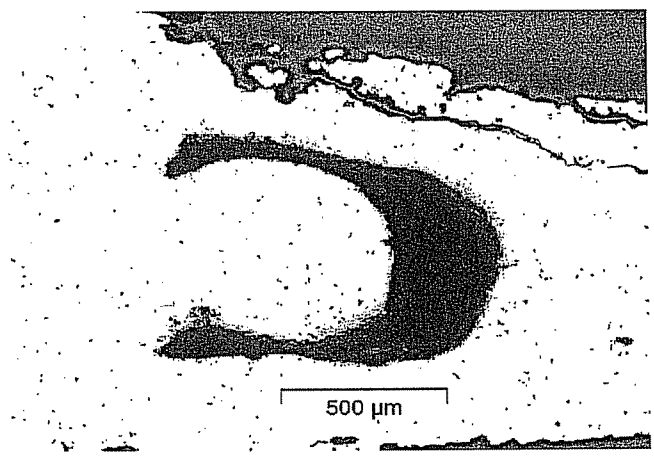

Figure 13: Feeding flaw, bar 13B, 50 times magnified, as polished

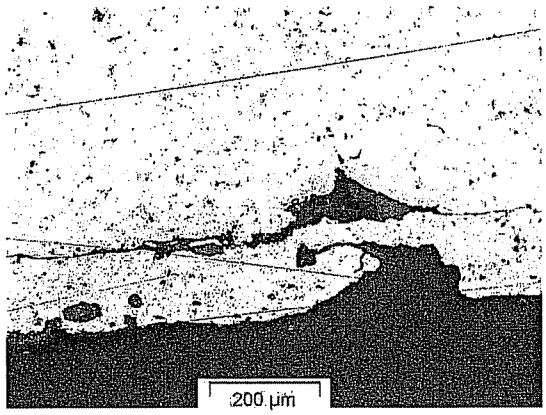

Figure 14: Clink, bar 13 A, 100 times magnified, as polished

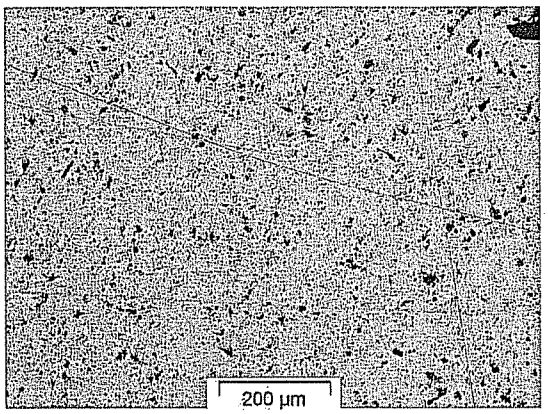

Figure 15: Bar 13C, 100 times magnified, as polished

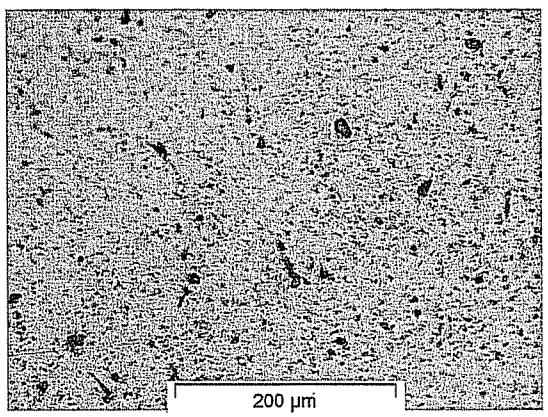

Figure 16: Bar 14A, 200 times magnified, etched by a 0.5% hydrofluoric acid attack

It was decided to subject one of the samples (bar 14 A, where A is referenced in figure 12) to the scanning electron microscope to know the nature of these inclusions.

3.3 Scanning electron microscope analysis

The scanning electron microscope analysis reveals the following facts:

- when oxygen is present, it is associated to silicon,
- in most of the inclusions, a silicon peak is visible, sometimes with other elements like carbon or iron.

In other words, inclusions are particles rich in silicon oxide and rich silicon particles.
We can hardly imagine these inclusions come from a solid state diffusion because the quantity of silicon of the alloy is very low, the density of inclusions very dense and the interface between the aluminum matrix and silicon would be totally different. Here, we have an empty zone between silicon and the matrix.
Now, an imperfect melting of silicon during the preparation of the alloy is possible: silicon has a melting point of about $1415°C$ against a melting temperature of about $650°C$ for aluminum.
The presence of silicon is likely to be explained as follows: rich silicon or silicon oxide particles are dragged by the liquid metal flow, but they do not perfectly wet it. Once in the mold, and as the solidification occurs, the particle leaves an empty zone around it because on the one hand it does not perfectly wet the metal (see figure 17), and on the other hand because of the matrix shrinkage (see figure 18).

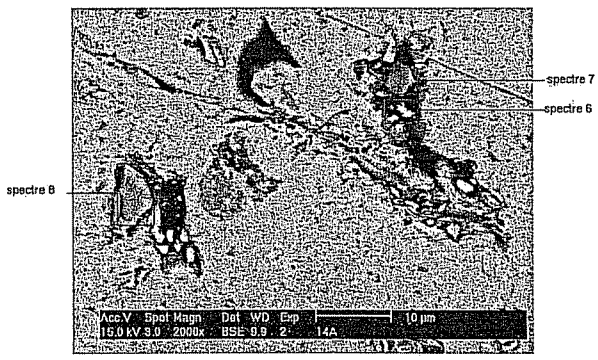

Figure 17: BSE picture of patch 2111

It is obvious that the low density of the rotor bars and the presence of inclusions have an impact on mechanical properties, by reducing the effective section of the rotor bar and by offering a path for crack propagation. It should also have an impact on conductivity, but unfortunately, no proper equipment was available to do a conductivity measurement. Let us mention that ceramic foam filters can be both an efficient and not so expensive way to prevent inclusions, as long as the contamination does not occur in the injection machine.

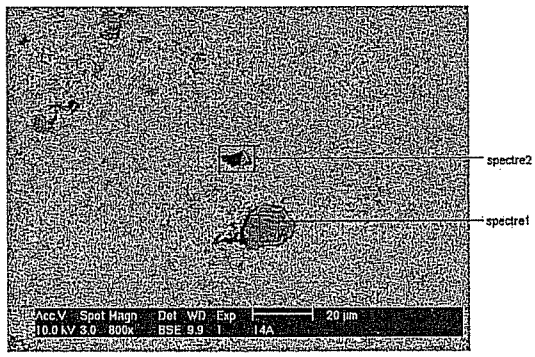

Figure 18: BSE picture of patch 111

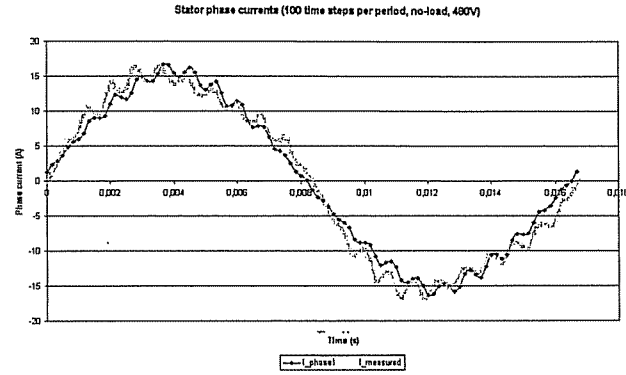

Figure 20: Stator phase current at no-load at 480 V

4 Simulation results and discussion

4.1 Introduction

In February and March 2004, in the frame of a training period, tests were carried out in WEG Motors Laboratory, (Jaraguá do Sul, Brazil). The machines used for the tests are sane cage motors (see 2.1 for the characteristics) and prototypes with one broken bar (see 1.2 for the manufacturing of these prototypes). The data recorded during these tests is compared in the following paragraphs to the computation results, considering no broken bars or one broken bar, no-load conditions (at different voltages) and rated load conditions.

4.2 One-pole model

The one pole model is used to validate the model of the motor with no broken bars. Let us first consider no-load conditions, under 150V and 480V voltages. Under a 480V voltage, the magnetic core of the motor is significantly saturated, which leads to a greater computation time. Figures 19 and 20 compare the recorded stator phase current with the recorded ones. One can observe that a good agreement is met.

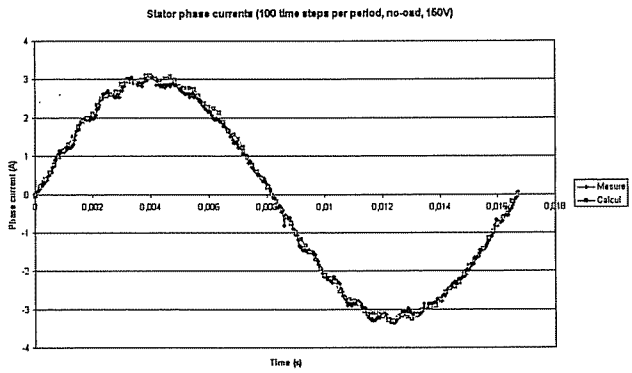

Figure 19: Stator phase current at no-load at 150V

We can now consider rated load conditions. As shown in figure 21, when considering only the temperature effect on conductivity, the computed phase currents are much higher than the recorded ones.

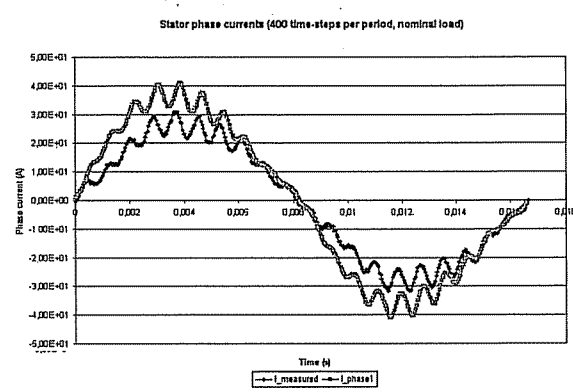

Figure 21: Stator phase current, straight cage motor at rated load at 440V

In order to check the computed phase current values, an equivalent scheme was used (see figure 22)[13].
In this scheme, the following elements are taken into account:

- the stator resistance R_s (Ω),
- the rotor resistance R'_r (Ω), referred to the stator,
- the magnetizing reactance X_m (Ω),
- the stator leakage reactance X_s (Ω),
- the rotor leakage reactance X'_r (Ω), referred to the stator.

The value of the stator resistance is chosen equal to 0.5 Ω, according to the measurements made. The value of the stator and rotor leakage reactance is obtained from the locked rotor test, dividing the value of their sum (1.4 Ω) into two. The value of the magnetizing reactance is estimated from a no-load test (line current 14 A, voltage 440V). It gives us a 54 Ω magnetizing reactance.
Let us now calculate a value for the rotor resistance, which is the sum of the rotor bar resistance and the

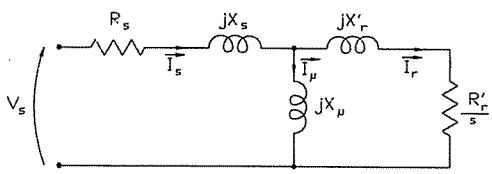

Figure 22: Equivalent scheme of the induction motor

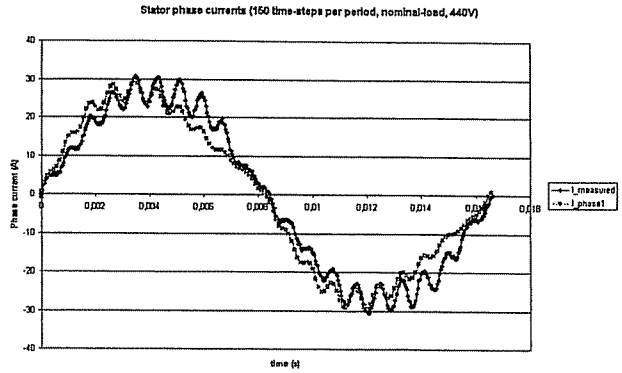

Figure 23: Stator phase current at rated load at 440V

two end-ring resistance [13]. The same value of conductivity as for the FE model is used: $\sigma = 28 \cdot 10^6$ S/m, which takes into account a warming of the rotor-bars up to a $80°C$ (conf. 2.3). We find that the rotor equivalent resistance which appears in the equivalent scheme is $R'_r \cong 0.42\Omega$.
Using the equivalent scheme, the effective value of the phase current at rated load and with a 440V supply voltage is 22.29 A, i.e. a 38.6A line current, which confirms the results of the FE model. Let us now consider the measured value of the line current: $32A$. In order to know which value of R'_r would give this line current value, a parametric study of R'_r was made. The results are given in the following table (table 2), where I_s is the rms stator phase current (see figure 8.10) and I_l the rms line current.

Table 2–Parametric study of phase current and line current as the rotor equivalent resistance varies

R'_r (Ω)	I_p (A)	I_l (A)
0.4	27.2	47.06
0.42	25.94	44.93
0.5	22.39	38.79
0.6	19.25	33.34
0.62	18.75	32.48
0.63	18.51	32.06
0.65	18.06	31.28

Only when the rotor resistance is taken equal to 0.62 Ω do we obtain an effective value of the phase current similar to the one measured (32 A). This means that the real rotor resistance value is about 48% higher than the resistance which is calculated without taking into account the material flaws (see above).
Computations were started again with a value of conductivity equal to $(18 \cdot 10^6$ S/m). The phase current curve is shown in picture 8.9. The computed phase current agrees well with the measured one.

4.3 Four-pole model

The goal of this work is to apply the FE model to straight cage motor having one broken bar. To this aim, a four-pole model was built, copying and rotating the geometry of the one pole model 3 times and imposing periodicity instead of anti-periodicity. Figure 24 shows the mesh of the four-pole model. The model was run during a few periods and the results compared to the ones of the one-pole model. They both gave the same results without broken bars, which means that the four-pole FE model is validated, in order to apply it to a one broken bar rotor. In this model, one broken bar is

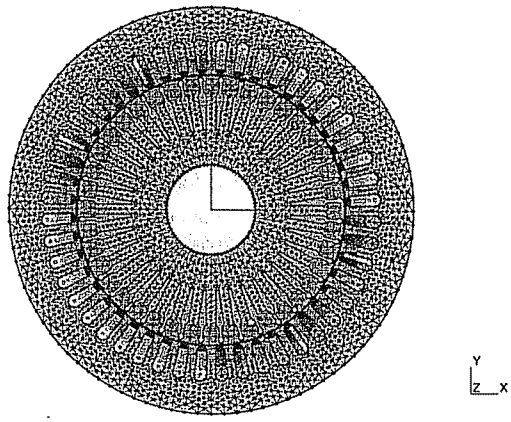

Figure 24: Mesh of the four pole model

simulated by specifying a very low value of conductivity for the first rotor bar (10^3 times less than for a healthy bar). In the rest of the section, the broken bar will be referred to "bar1".
A 150 time-steps per period computation was done at no-load. Stator phase currents is shown in figure 25.
The computed current amplitude agrees well with the measured one.
Let us now consider a rated-load computation with 150 time-steps per period. Flux lines are shown in figure 26. Considering the counterclockwise direction of rotation of the rotor as positive, the bar situated ahead of the broken one (let us call this bar "bar2") is characterized by a rise in the flux line concentration. Therefore, the current which flows through bar 2 should increase

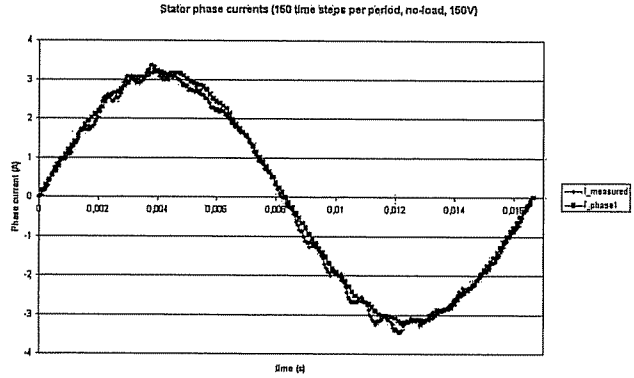

Figure 25: Stator phase current at no-load at 150V

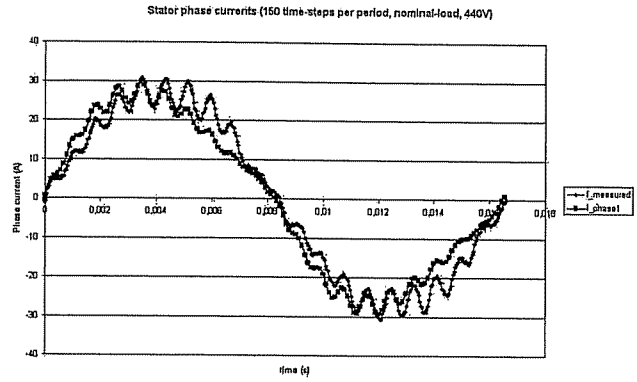

Figure 27: Stator phase current at rated load, 440V

more than the current in the other rotor bars when bar 1 is broken. As a result, the Joule effect (and hence the stresses due to thermal wear), the stresses due to Laplace force,... should increase in bar 2. This result agrees well with [11]. A stator phase current is shown in figure 27. It agrees reasonably well with the measured current.

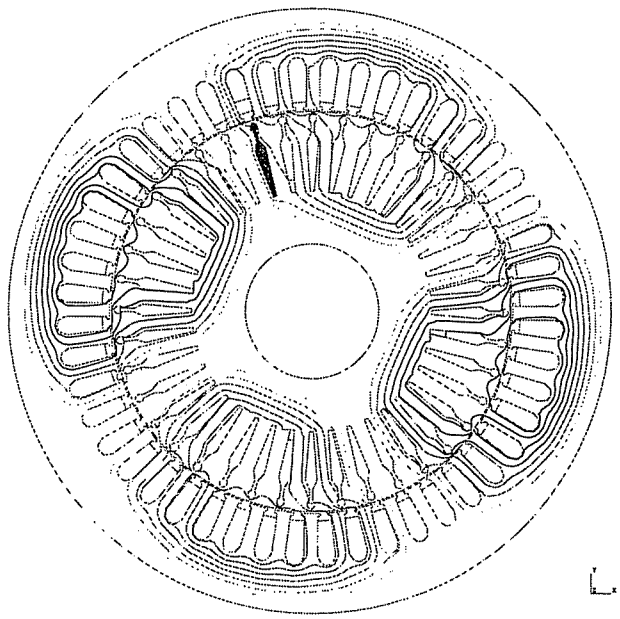

Figure 26: Flux lines at rated load 20 periods

5 Summary and Conclusions

For what the metallurgical analysis of the aluminum alloy of the rotor bars concerns: the micrographies showed a very high density of inclusions in the aluminum matrix, shrinkage, as well as cracks. The scanning electron microscope gave us the composition of the inclusions: most of them are rich silicon particles, sometimes silicon oxide particles, with carbon or iron tracks. All these non-conductive inclusions have a very negative impact on conductivity, as well as on the mechanical properties, reducing the effective section and offering a path for crack propagation.

For what the modelling of the no-broken bar motor concerns: no-load simulations gave good results. For the load modelling, the influence of the rotor is more important. It appeared that the influence of the material flaws was not negligible. The equivalent scheme used allowed to estimate that the real rotor resistance was about 50% higher than the rotor resistance calculated considering only the temperature effect on the conductivity of the bars. Once the effect of material flaws taken into account, the simulation results were good.

For what the modelling of a broken rotor bar induction motor concerns: the previously determined conductivity was used and led to good simulation results. The field perturbation associated with a broken rotor bar produces a concentration of flux near the bar ahead of the broken one, considering the counterclockwise direction of rotation of the rotor. This flux concentration results in higher current values –and hence in higher stresses– in the bar ahead of the broken one. This result is in agreement with [11].

The high purity degree, and hence high conductivity properties, of the costly 99.7 % aluminum alloy injected could be better exploited. Not only do the injection flaws seriously diminish conductivity, but they also diminish the mechanical properties of the alloy, leading to an easier breaking of the bars. It would be recommended to detect the step of the process at which contamination by particles occur. If the contamination occurs before the pouring of molten aluminum in the injection machine, a filtering of the liquid metal bath is possible (see chapter 7). Also, this measure must be accompanied by a revision of the injection process (for example with an experimental variation of the injection parameters), in order to avoid the shrinkages.

Studying the influence of broken rotor bars is one step, but discovering the reasons why they appear in order to avoid them is the true finality of the engineer's job.

Acknowledgments

I want to express my very warm thanks to Dr.ir. Johan Gyselinck, Dr.ir. Jacqueline Lecomte and WEG Motores collaborators. Many thanks to the MMS Department crew, to the Electrical Engineering Department crew and to Dr.ir. Jean-Louis Lilien.

References

[1] S. L. Nau, "The Influence of the Skewed Rotor Slots on the Magnetic Noise of Three-Phase Induction Motors," *EMD97 1-3 September 1997* , Conference Publication No.444, IEE1997.

[2] R. L. Nailen, "The Significance of Skew P.E., " *Electrical Apparatus* , January 1988.

[3] J. Gyselinck and X.M. López-Fernandez, "Inclusion of inter-bar currents in multi-slice FE modelling of induction motors-influence of inter-bar resistance and skew discretisation " *Proceedings of the 16th International Conference on Electrical Machines (ICEM2004)* , Cracow, Poland, 5-8 September 2004, pp. 621-622, extended paper (790) on CD-ROM.

[4] H. Razik, "Ah! La machine asynchrone, que de soucis quand elle tombe en panne!!!," , Université Henri Poincaré Nancy 1.

[5] W.T. Thomson, S.J. Chalmers, D. Rankin, "An On-Line, Computed-Based Current Monitoring System for Rotor Fault Diagnosis in 3-Phase Induction Motors," *Turbomachinery international*, November/December 1987, p17.

[6] Pavel N. Dobrodeyev, Sergey A. Volokhov, Alexander V. Kildishev, J.A. Nyenhuis, "Method for Detection of Broken Bars in Induction Motors," *IEEE Transactions on Magnetics*, vol. 36, NO. 5, September 2000.

[7] K. Rae Cho, Jeffrey H, Lang, "Detection of Broken Rotor bars in Induction Motors Using State and Parameter Estimation," *IEEE Transactions on Industry Applications*, Vol. 28, No.3, May/June 1992.

[8] Nagwa M. Elkasabgy, Anthony R. Eastham, Graham E. Dawson, "Detection of Broken Bars in the Cage Rotor on an Induction Machine," *IEEE Transactions on Industry Applications*, Vol. 28, No.3, January/February 1992.

[9] J. Mimonfared, H. Kelk, S. Nandi, "A Novel Approach for Broken-Rotor-Bar Detection in Cage Induction Motors," *IEEE Transactions on Industry Applications*, Vol. 35, No.5, September/October 1999.

[10] Muller G.H., Landy C.F., "Vibration produced in squirrel cage induction Motors having broken rotor bars and interbar currents," *ICEM 1994* , vol 3.

[11] X. M. López-Fernandez and Marius Piper, "Magnetodynamic Performance in Cage Induction Motors with a Broken Bar," *ISEF2003* .

[12] S. Guérard, *"FE modelling of an asynchronous motor with one broken bar, comparison with the data recorded on a prototype and material aspects, Master work"* , University of Liège, 2004.

[13] J. Gyselinck, *"Twee Dimensionale Dynamische Eindige-Elementenmodellering van Statische en Roterende Elektromagnetische Energieomzetters"*, Doktoraatsthesis, Universiteit Gent, 2000 .